A Revised Cloud Overlap Scheme for Fast Microwave Radiative Transfer in Rain and Cloud

ALAN J. GEER AND PETER BAUER

European Centre for Medium-Range Weather Forecasts, Reading, United Kingdom

CHRISTOPHER W. O'DELL

Department of Atmospheric Science, Colorado State University, Fort Collins, Colorado

(Manuscript received 11 December 2008, in final form 29 April 2009)

ABSTRACT

The assimilation of cloud- and precipitation-affected observations into weather forecasting systems requires very fast calculations of radiative transfer in the presence of multiple scattering. At the European Centre for Medium-Range Weather Forecasts (ECMWF), performance limitations mean that only a single cloudy calculation (including any precipitation) can be made, and the simulated radiance is a weighted combination of cloudy- and clear-sky radiances. Originally, the weight given to the cloudy part was the maximum cloud fraction in the atmospheric profile. However, this weighting was excessive, and because of nonlinear radiative transfer (the ''beamfilling effect'') there were biases in areas of cloud and precipitation. A new approach instead uses the profile average cloud fraction, and decreases RMS errors by 40% in areas of rain or heavy clouds when ''truth'' comes from multiple independent column simulations. There is improvement all the way from low (e.g., 19 GHz) to high (e.g., 183 GHz) microwave frequencies. There is also improvement when truth comes from microwave imager observations. One minor problem is that biases increase slightly in mid- and upper-tropospheric sounding channels in light-cloud situations, which shows that future improvements will require the cloud fraction to vary according to the optical properties at different frequencies.

1. Introduction

The small-scale variability of cloud and precipitation must be carefully modeled in order to get accurate simulations of atmospheric radiative transfer. For example, the amount of overlap between different cloud layers can strongly affect quantities such as heating rates and the earth's albedo (e.g., Morcrette and Fouquart 1986; Morcrette and Jakob 2000). At microwave frequencies, the nonlinear dependence of radiance on hydrometeor amount causes a ''beamfilling effect'' in satellite observations (e.g., Kummerow 1998). Here, even when two fields of view contain the same mass of rain or cloud, variations in fractional cloudiness can cause large differences in measured radiances.

Rain- and cloud-affected microwave radiances are assimilated at the European Centre for Medium-Range Weather Forecasts (ECMWF; Bauer et al. 2006a,b), improving forecasts of tropical moisture and wind (Kelly et al. 2008). However, large biases between simulated and observed brightness temperatures (TBs) remained in cloudy and rainy areas, even after improvements made by Geer et al. (2008). A major part of the remaining bias was likely a result of inadequate treatment of subgrid cloud variability in the radiative transfer simulations. This paper tests a revised approach that substantially reduces biases between model and observations.

Typically, the only knowledge that a GCM has of subgrid cloud variability is the cloud fraction at each layer. Traditionally, a ''maximum random'' cloud overlap has been used when modeling subgrid-scale variability in radiative transfer calculations (Geleyn and Hollingsworth 1979). Vertically continuous cloud layers are overlapped by the maximum possible; however, where there is a gap between cloud layers, they are overlapped by a random amount. Ground- and space-based radar observations

Corresponding author address: Alan Geer, European Centre for Medium-Range Weather Forecasts, Shinfield Park, Reading, RG2 9AX, United Kingdom.
E-mail: alan.geer@ecmwf.int

DOI: 10.1175/2009JAMC2170.1

have shown that maximum overlap is valid over short vertical distances, and there is a transition to random overlap over about 2 km (Hogan and Illingworth 2000; Mace and Benson-Troth 2002; Barker 2008). However, the atmospheric state is important, and maximum overlap occurs preferentially in strong ascent and in convectively unstable conditions (Naud et al. 2008).

To represent subgrid variability in radiative transfer simulations, an independent column approximation (ICA) is often used. Here, the grid box is divided into a set of independent subcolumns with radiative transfer done separately for each. Cloud distributions in each subcolumn are assigned according to an overlap scheme or some other method. Within each layer of a subcolumn, cloud is either wholly present or wholly absent. However, this approach does not take into account 3D effects, such as emission from the sides of clouds and precipitation (e.g., Weinman and Davies 1978). The ICA approach is used as a reference here, following O'Dell et al. (2007), who performed a similar study to this one and showed the ICA was acceptable.

The computational cost of assimilating rain- and cloud-affected microwave radiances is very large. At ECMWF, a new direct approach became operational in March 2009, with the microwave imagers taking about 10% of the total resources used for assimilation, mainly because of scattering radiative transfer. In order to reduce the cost even this far, only one cloud- or rain-affected subcolumn can be simulated per observation. However, this makes it difficult to correctly account for subgrid cloud and rain variability (Bauer et al. 2006c).

It would be too expensive to use a method such as the ICA operationally, a much faster approach is the Monte Carlo ICA (McICA; Pincus et al. 2003), which has revolutionized the calculation of broadband fluxes and heating rates in GCMs, including the ECMWF (Morcrette et al. 2008). However, because it introduces large random errors in simulations at any one frequency, it is not appropriate for the simulation of satellite observations. Recently, O'Dell et al. (2007) developed an "optimal" cloud overlap for microwave radiative transfer that performs near identically to the ICA and needs only two or three scattering calculations. But, for the moment, this is still too expensive for use at ECMWF; therefore, in this study we search for an improved cloud overlap using just one calculation.

This paper will evaluate different versions of the radiative transfer code in a wide variety of different atmospheric situations, and it will compare the simulated TBs both with observations and with reference simulations. The study is done in the context of the observation minus forecast statistics, which are a main output of an operational numerical weather prediction (NWP) system, along with analyses and forecasts.

2. Method

a. ECMWF assimilation system

ECMWF produces routine global analyses and 10-day forecasts from an assimilation system based on an atmospheric model with a semi-Lagrangian, spectral formulation. The model has 91 levels from the surface to an altitude of 80 km and a T799 horizontal resolution, corresponding to about 25 km (information available online at http://www.ecmwf.int/research/ifsdocs/). Global analyses of wind, temperature, surface pressure, humidity, and ozone are produced twice daily using a four-dimensional variational assimilation system (4D-Var; Rabier et al. 2000) with a 12-h time window. Assimilated observations include in situ conventional data, satellite radiances from polar orbiters [from instruments such as the Advanced Microwave Sounding Unit (AMSU) and the Infrared Atmospheric Sounding Interferometer (IASI)], geostationary radiances, satellite-derived atmospheric motion vectors, and surface winds from scatterometers.

From June 2005 to March 2009, microwave imager observations were assimilated, over oceans only, in two separate streams. Clear-sky observations were assimilated as radiances directly in 4D-Var; those identified as affected by cloud and rain were assimilated using a 1D + 4D-Var procedure (Bauer et al. 2006a,b; Geer et al. 2008). Data from Special Sensor Microwave Imager (SSM/I), Tropical Rainfall Measuring Mission (TRMM) Microwave Imager (TMI), and Advanced Microwave Scanning Radiometer for Earth Observing System (AMSR-E) were assimilated in all weather conditions. Data from Special Sensor Microwave Imager/Sounder (SSMIS) were assimilated in clear-skies only, because the observation data we receive have been averaged spatially (Bell et al. 2008), which eliminates the small-scale rain and cloud features. Our experiments are based on this system, although here we will use only SSM/I and SSMIS.

b. SSM/I and SSMIS instruments

A series of SSM/I instruments has been flown on the Defense Meteorological Satellite Program (DMSP) satellites from 1987 until the present day (Hollinger et al. 1990). SSM/I utilizes a conical scanning technique which gives all observations the same zenith angle, 53.1°. Here, we use observations from DMSP *F13* and *F14* satellites, and corresponding simulations have been created using the first-guess (FG) model fields. SSM/I has seven channels at frequencies from 19 to 85 GHz, where the atmosphere is semitransparent in clear skies and most absorption comes from total column water vapor, due to both water vapor continuum absorption and the 22-GHz line. In cloudy skies, the lower-frequency

channels are sensitive to rain and cloud water and the higher-frequency channels are sensitive to snow and cloud ice as well. SSM/I observations have been corrected at ECMWF for the scan-dependent biases found by Colton and Poe (1999).

To extend our study to sounding channels and to higher frequencies, we have also simulated TBs for seven channels of the SSMIS instrument on DMSP *F16* satellite (Kunkee et al. 2008). Three of these were oxygen band temperature sounding channels, at similar frequencies to those of AMSU-A: 50.3, 52.8, and 53.6 GHz (all vertically polarized). Weighting functions progress from the lower to the upper troposphere, and we have ignored the stratospheric oxygen band channels. The other four channels were similar to those found on AMSU-B, being at 150 ± 1 GHz (a window channel) and in the 183.31-GHz water vapor line at 183.31 ± 6.6, 3, and 1 GHz, sensing water vapor from the lower to the upper troposphere. However, as mentioned earlier, real SSMIS observations were unsuitable for comparison [see Figs. 3 and 4 of Bauer et al. (2006c) for further details on the information content of SSM/I and SSMIS].

c. Scattering radiation code

The Radiative Transfer Model for the TIROS Operational Vertical Sounder (RTTOV; Eyre 1991; Saunders 2008) includes a module that provides multiple-scattering radiative transfer calculations at microwave frequencies (RTTOV-SCATT; Bauer et al. 2006c). It is used operationally in the assimilation of rain- and cloud-affected radiances at ECMWF (Bauer et al. 2006a) and experimentally by many others (e.g., Deblonde et al. 2007).

RTTOV-SCATT uses the delta-Eddington approach (Joseph et al. 1976), which gives reasonable results when simulating the radiances measured by microwave radiometers (Smith et al. 2002). Scattering parameters are precalculated using Mie theory and tabulated as a function of frequency, temperature, and hydrometeor type and density. The most important inputs to RTTOV-SCATT are the surface skin temperature and winds and the vertical profiles of pressure, temperature, moisture, cloud liquid water and ice, rain and snow fluxes, and cloud cover. Cloud overlap approaches are described in section 3.

d. Experiment setup

Using the framework of the 1D + 4D-Var rain- and cloud-affected assimilation, SSM/I and SSMIS radiances were simulated using FG forecasts as input. The FG is a short-range (up to 12 h) forecast, initialized from the previous analysis, and it is used to provide the background state for data assimilation. FG forecasts were generated for a period of 20 days, from 1 to 20 August 2007, based on a modified version of cycle 32r3 of the ECMWF assimilation system and using a slightly reduced horizontal resolution of T511.

Forward radiative transfer simulations were made at every model grid point and time step where an SSM/I observation was available within 10 km of the grid-point center. The SSM/I field of view is 70 km by 45 km at 19 GHz, compared to a model gridbox size (at T511) of 40 km by 40 km. The model time step is 15 min. SSM/I field of view and model grid boxes will be considered equivalent; this is an assumption that has worked well for operational rain and cloud assimilation at ECMWF.

For improved accuracy, inputs to the radiative transfer code came directly from the FG model rather than the simplified 1D operators normally used in rainy 1D + 4D-Var assimilation. SSM/I observations were restricted to latitudes between 60°N and 40°S and the ocean only, avoiding land and sea ice surfaces. Latitudes poleward of 40°S were excluded as a result of a bias problem that will be explained later. All valid observations were used, including those normally sent through the ''clear'' assimilation stream. In other words, all sky conditions, whether clear, cloudy, or rainy, were included in the comparisons. In this way, the passive monitoring experiment produced the set of 4.2 million model profiles, radiative transfer simulations, and collocated SSM/I observations on which this study is based.

3. Cloud overlap

Table 1 lists the different cloud overlap schemes to be tested; these will be described in more detail in the following sections. The original (2C) and revised (2R) RTTOV-SCATT cloud overlap schemes have two subcolumns: one for the clear and one for the cloudy part of the grid box. The clear subcolumn takes into account only gaseous absorption, and the radiative transfer is computationally very fast; the cloudy subcolumn takes into account cloud, precipitation, and scattering and is much slower. The optimal approach of O'Dell et al. (2007), in the 2O configuration tested here, uses two subcolumns with scattering radiative transfer and hence has roughly twice the computational cost of 2C or 2R. The reference model (20ICA) has 20 subcolumns, all of which use scattering.

a. Simple schemes

RTTOV-SCATT calculates the all-sky brightness temperature TB_{allsky}, which depends on the overall cloud fraction C_{tot} as follows:

TABLE 1. Cloud overlap approaches to be tested.

Name	Subcolumns: Scattering	Subcolumns: Clear	Cloud overlap
2C	1	1	C_{max} weighting (original RTTOV-SCATT scheme)
2R	1	1	C_{av} weighting (new RTTOV-SCATT scheme)
2O	2	0	O'Dell et al. (2007)
20ICA	20	0	Maximum-random

$$\mathrm{TB}_{\mathrm{allsky}} = (1 - C_{\mathrm{tot}}) \times \mathrm{TB}_{\mathrm{clear}} + C_{\mathrm{tot}} \times \mathrm{TB}_{\mathrm{cloudy}}, \quad (1)$$

where $\mathrm{TB}_{\mathrm{clear}}$ and $\mathrm{TB}_{\mathrm{cloudy}}$ are the brightness temperatures of the clear and cloudy subcolumns, respectively. Input hydrometeor profiles from the model (cloud ice and water content; rain and snow flux) are representative of the gridbox average. To get the cloudy subcolumn density or flux w_i^*, at model level i for a given hydrometeor type, the input w_i is rescaled using the overall cloud fraction C_{tot}:

$$w_i^* = \frac{w_i}{C_{\mathrm{tot}}}. \quad (2)$$

In the original implementation of RTTOV-SCATT (Bauer et al. 2006c) and in previous, closely related schemes (e.g., Chevallier and Bauer 2003), C_{tot} was set to the maximum cloud fraction in the profile, C_{max}:

$$C_{\mathrm{max}} = \max(C_i), \quad (3)$$

where C_i is the input cloud fraction on model level i. However, it is quite typical that the maximum cloud fraction in a profile might be representative of only a thin layer, perhaps a cirrus cloud, convective outflow, or a low-level cloud deck. But these may only have a small optical depth in the microwave. On the other hand, if a deep convective cell is present it may occupy just a small part of the gridbox area, but the heavy cloud and precipitation it contains will have a strong local effect on microwave radiation. Figures 1a,b illustrate this situation, as modeled with maximum-random overlap and the original RTTOV-SCATT scheme, respectively. For simplicity, only the cloud is shown, but precipitation overlap is equally important.

It is here that the ''beamfilling effect'', (i.e., the nonlinear response of TB to hydrometeor content) becomes important. To illustrate this, Fig. 2 shows a regression between liquid water path (LWP; kg m^{-2}) and SSM/I 37-GHz horizontally polarized TB (T^{37h}; K), derived by Karstens et al. (1994, algorithm 2, their Table 3):

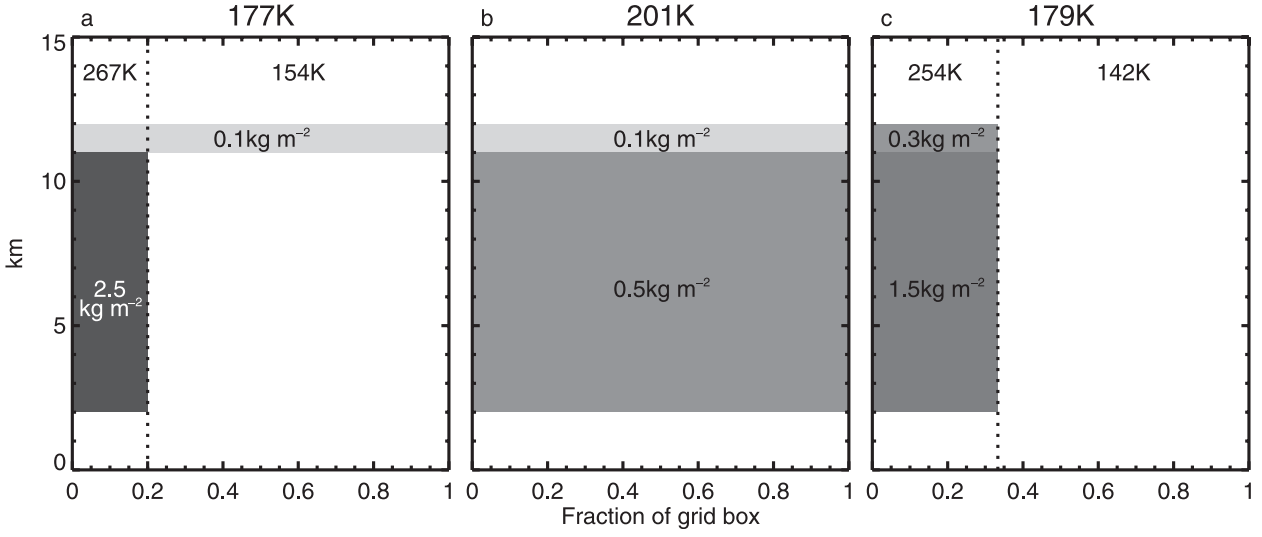

FIG. 1. Illustrations of different cloud overlap techniques: (a) maximum-random overlap with unlimited independent columns (although only two are required here; note also that maximum overlap would produce identical results in this case, because there are no separated cloud layers); (b) C_{max} overlap as used in RTTOV-SCATT; and (c) proposed C_{av} overlap. Gray boxes represent clouds with the stated part-column cloud LWPs. Averaged over the whole grid box, the clouds have the same mass per unit area. The headline brightness temperature is the average over the whole grid box; others apply to the individual columns. Unlike in a real model, vertical levels have been allocated to fit the cloud structure.

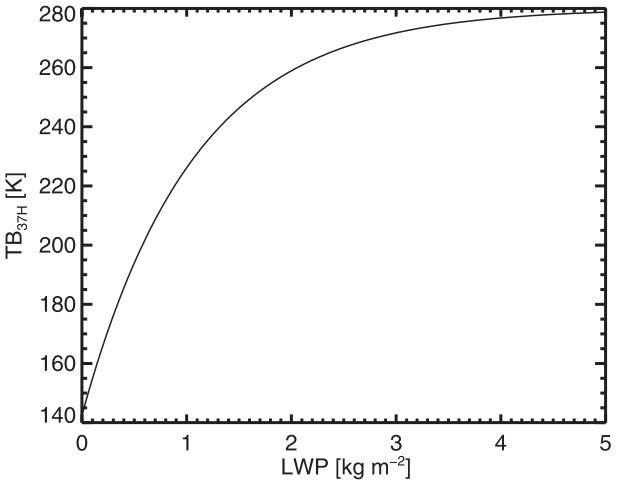

FIG. 2. Karstens et al. (1994) second LWP regression.

$$T^{37h} = 280 - \exp\left(\frac{\text{LWP} - 5.2524}{-1.06678}\right). \quad (4)$$

It can be seen that, at higher liquid water paths, TBs saturate. The dependence of TB on rain has a similar shape (e.g., Fig. 3 of Kummerow 1998). Therefore, it will be problematic when the cloud and precipitation from that convective core, which should be contained within the locally applicable cloud fraction (0.2 here), is spread out through the whole grid box, as would happen in the original RTTOV-SCATT scheme when $C_{\text{tot}} = C_{\text{max}} = 1$ (Fig. 1b). The rain and precipitation from the convective core will have a much greater influence on the gridbox TB than it should. At low microwave frequencies where cloud liquid water and rain absorption is much stronger than any scattering effect, this will result in excessively high simulated TBs.

The numbers given in Fig. 1 show some possible values for cloud liquid water and the result of using Eq. (4) to simulate the brightness temperature. We have ignored the presence of rain and pretended that all clouds are in the liquid phase. The ICA needs only two columns in this example: the convective core with LWP = 2.5 + 0.1 = 2.6 kg m^{-2} and the outflow cloud with LWP = 0.1 kg m^{-2}. Using this, the TB observed in channel 37h would be $T^{37h} = 0.2 \times 267 + 0.8 \times 154 = 177$ K. As compared with this, the original RTTOV-SCATT overlap [Eqs. (1) and (2)] would give a single, cloudy column, with LWP = 0.6 kg m^{-2}, and would give an erroneously high TB of 201 K. We suspected that such an effect could explain the biases observed in the FG departures in the assimilation of rainy and cloudy SSM/I observations at ECMWF.

One possible solution to these problems would be to choose a value for C_{tot} that is more representative of the actual radiative transfer. An initial choice was simply to calculate an average cloud fraction over the whole profile, weighting by the total hydrometeor amount:

$$C_{\text{av}} = \frac{\sum_i (l_i + i_i + r_i + s_i)\Delta z_i C_i}{\sum_i (l_i + i_i + r_i + s_i)\Delta z_i}, \quad (5)$$

where, l_i, i_i, r_i, and s_i represent respectively the cloud liquid, cloud ice, rain, and snow densities (kg m^{-3}) and Δz_i is the layer thickness in meters. It is implicitly assumed that the cloud fraction also applies to the rain and snow amounts. We have investigated using a separate precipitation fraction, which would be more appropriate for levels where rain or snow has fallen out of a cloud, but the effect on our results is not large. Taking the part-column LWP ($=l_i\Delta z_i$) from Fig. 1a, $C_{\text{av}} = (0.5 \times 0.2 + 0.1 \times 1)/(0.5 + 0.1) = \frac{1}{3}$, and Eq. (1) now gives a TB of 179 K (Fig. 1c), much closer to that estimated with the ICA.

We have deliberately stepped back from trying to decide the effective cloud fraction by using a measure that is more precisely representative of the radiative transfer in a particular satellite channel. We would need to account for the fact that the radiative effects of cloud, rain, and snowfall change depending on the frequency. Also, the vertical weighting should be different in a window channel compared to a sounding channel, where the lower parts of the troposphere may be optically thick and we should only consider the upper parts of the profile. The hope is that a simple approach, like Eq. (5), can be applied to all channels as a first order improvement to the radiative transfer. As shown in the following sections, this technique does provide substantial improvements when applied to the real RTTOV-SCATT, but a further refinement of the technique would be to chose a separate C_{tot} for each channel, perhaps based on precomputed weighting functions. However, this is not a straightforward thing to implement in the radiative transfer scheme.

Figures 3 and 4 show means of C_{max} and C_{av} in the ECMWF profiles, illustrating that situations with widespread thin cloud are quite typical. The discrepancy between C_{max} and C_{av} is largest in the ITCZ, where C_{max} is roughly 2.5 times larger. In these regions, the main mass of hydrometeors is found in relatively localized convective cores. Subtropical stratocumulus regions near the east coasts of Africa and South America show the least differences between C_{max} and C_{av}. Here, the air is usually subsiding at upper levels and cirrus or other clouds are less likely; the main mass of cloud comes from boundary layer maritime stratocumulus.

A minor complication arises because the rain and snow inputs to RTTOV-SCATT are in terms of flux

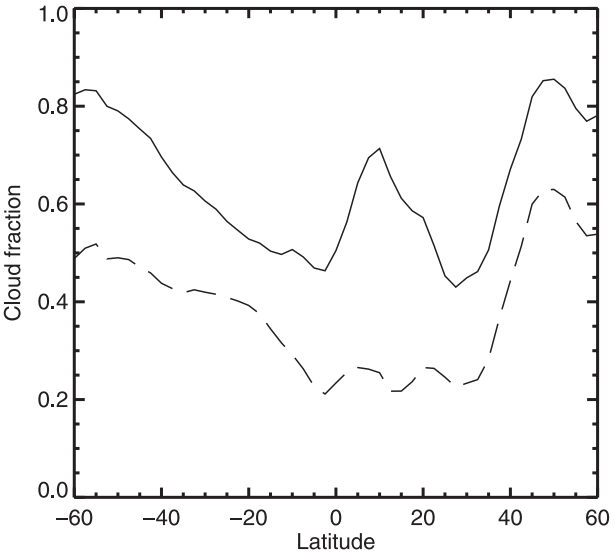

FIG. 3. Zonal mean average (dashed) and maximum (solid) cloud fraction in the ECMWF profiles.

(kg m^{-2} s^{-1}), but there is a nonlinear conversion to density (kg m^{-3}) that is used in the calculations. By assuming exponential size distributions for both rain and snow, constant density with size, and a certain distribution of fall speeds, the following relation between precipitation rate[1] (PR; mm h^{-1}) and water content (WC; g m^{-3}), has been derived:

$$\mathrm{PR} = a \times \mathrm{WC}^{b}, \tag{6}$$

where coefficients a and b are given in Table 2. By using different coefficients, the relation can be applied either to link rain rate and liquid water content or snow rate and frozen water content.

In scheme 2C, Eq. (2) is applied to the rain and snow fluxes, but in 2R it is applied to the densities. This was chosen because it is the densities that are most directly related to the radiative transfer. The effect on the 2R brightness temperatures of scaling the fluxes versus scaling the densities can be as much as +0.5 or −1.5 K in channel 37v in some cloudy and rainy areas. However, this is minor in comparison with the overall differences between 2C and 2R.

b. Reference model

20ICA uses 20 equal-sized subcolumns, with clouds allocated according to maximum-random overlap and precipitation allowed to fall out of cloud into noncloudy areas beneath. This is consistent with the overlap approach used in the ECMWF moist physics, though not with the ECMWF radiation scheme, which uses generalized cloud overlap (Morcrette et al. 2008). It is a future task to move to generalized cloud overlap throughout. Each subcolumn is simulated using RTTOV-SCATT, with the restriction that the cloud fraction in any layer can only be 0 or 1. O'Dell et al. (2007) compared this approach with a more accurate 3D model, and they argued that the errors in the 20ICA are acceptably small for this kind of study.

c. Optimal approach

The optimal approach of O'Dell et al. (2007) is also tested here, because it is a candidate for data assimilation use in the future. It is compared to real observations for the first time here. The optimal approach attempts to replicate the performance of the ICA, but using a far smaller number of subcolumns. The idea is that subcolumns are binned together where they have similar optical properties at the frequencies of interest.

First, cloud and precipitation amounts are allocated to 32 equal-size subcolumns by using maximum overlap, but with precipitation allocated using the same approach as described earlier. Then, the slant column optical depth at 37 GHz (τ_j^{37}) is estimated in each subcolumn j as

$$\tau_j^{37} \simeq \sec\theta\left(G + \sum_i k_{ij}^{37}\Delta z_i\right), \tag{7}$$

where $G = 0.02$ and roughly accounts for gas absorption, θ is the observation zenith angle, and k_{ij}^{37} is the volume extinction coefficient and is estimated as

$$k_{ij}^{37} \simeq 3598 r_{ij}^{1.15} + 1031 s_{ij}^{1.35} + 237 l_{ij}. \tag{8}$$

In the actual calculation, this is done in terms of rain and snow fluxes and cloud water density, but here we have transformed the precipitation fluxes to density (see earlier), and all are in units of kilograms per cubic meter, for comparison to Eq. (5) [note that the snow term has been slightly altered from O'Dell et al. (2007)].

Next, the subcolumns are grouped into a chosen, smaller number of bins, according to their optical depth τ_j^{37}. The cloud and precipitation profile for each bin is an equally weighted average over its subcolumns. A single radiative transfer simulation (using RTTOV-SCATT) is done for each bin, again assuming cloud cover is either 0 or 1 in each layer. We have chosen to use two bins here, because this is the most likely configuration we would use in data assimilation. The final TB is the average over the bins, weighted by the fraction of the grid box that they represent.

[1] In our calculations, the conversion of flux (kg m^{-2} s^{-1}) to a precipitation rate (mm h^{-1}) assumes the density of snow to be 100 kg m^{-3} and the density of water to be 1000 kg m^{-3}.

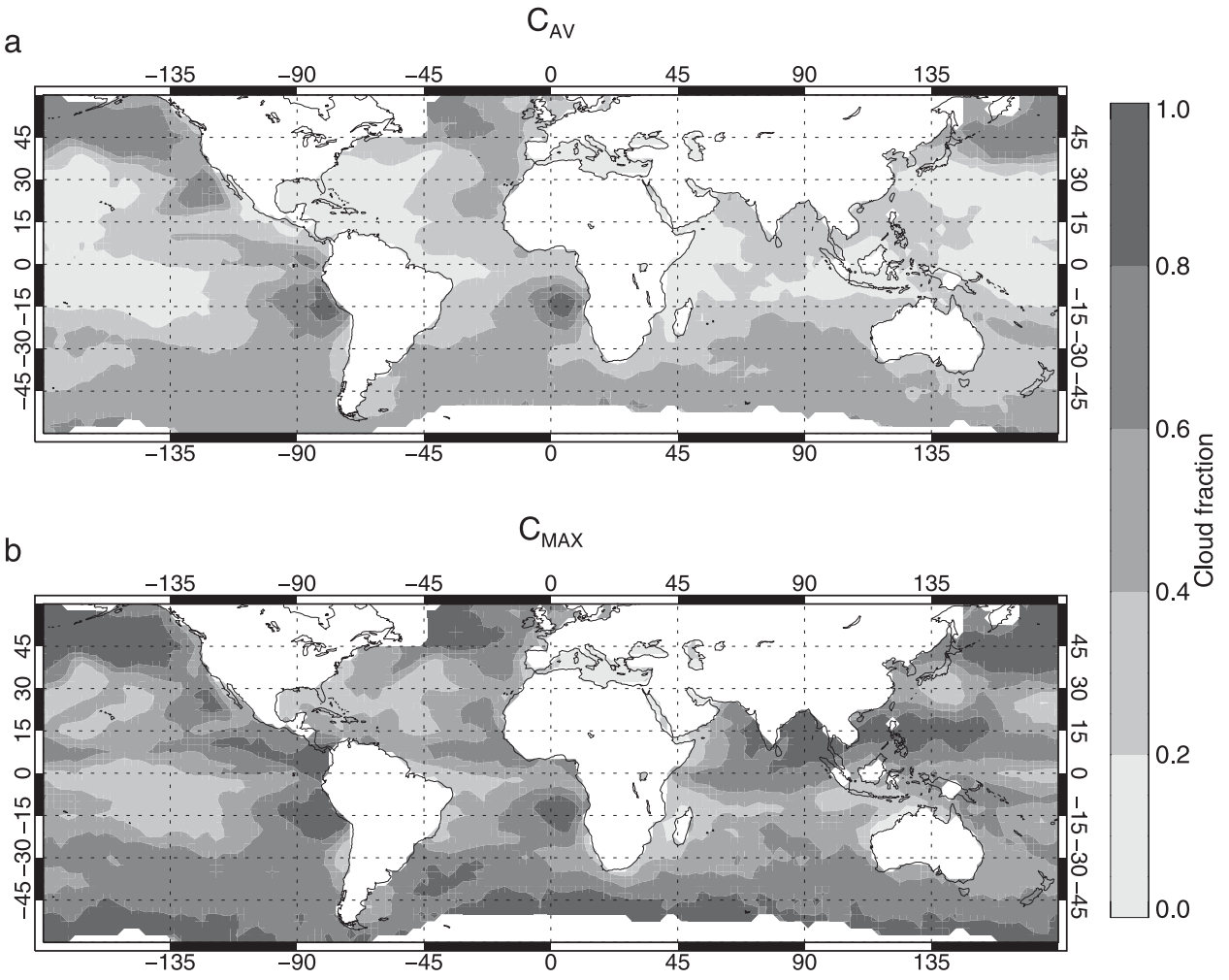

FIG. 4. Mean cloud fraction in the ECMWF profiles, binned in 2.5° by 2.5° boxes: (a) average and (b) maximum. White areas have no observations that pass our screening criteria.

Note that the choice of 37-GHz optical depth as a proxy for TBs of all frequencies means that the effects of scattering are ignored when choosing the bins, despite the fact that these effects are important at higher frequencies. Also, this will be incorrect for sounding channels with weighting functions peaking higher in the troposphere. As discussed for the 2R approach, a future refinement should be to assign different bins at different frequencies, according to the variation of optical properties.

4. Results

The set of profiles has been divided into two samples. The first sample is representative of rainy and heavy cloud areas, and for convenience it will be referred to simply as rainy. This sample contains all profiles where either the 2C simulations or the observations show a 37-GHz polarization difference of less than 40 K (e.g., Petty 1994). This selects 463 093 profiles. The second sample contains the other 3.75 million profiles, and it is representative of lighter cloud and clear-sky conditions. Only about 20% of ECMWF profiles have an LWP less than 0.01 kg m^{-2}, so the majority of profiles contain cloud with nonnegligible radiative effect. True clear-sky conditions are not affected by the choice of cloud overlap scheme, but it makes little difference to the results whether clear-sky profiles are included in the cloudy sample.

TABLE 2. Coefficients for Eq. (6), which links precipitation flux and density.

	a [mm h^{-1} (g m^{-3})$^{-1}$]	b
Rain	20.89	1.15
Snow	29.51	1.10

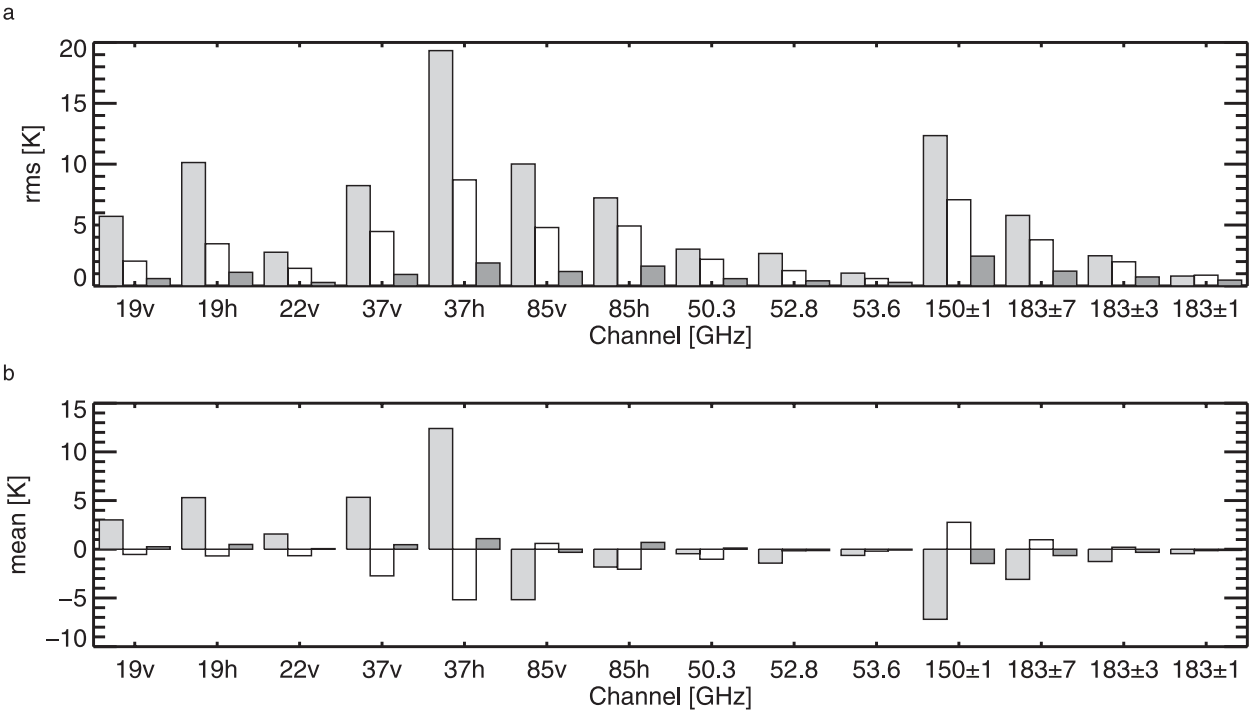

FIG. 5. (a) RMS and (b) mean errors in 2C (light gray), 2R (white), and 2O (dark gray) simulated TBs, as compared with the 20ICA simulations, for the rainy-sky sample.

a. Independent column calculations as truth

In this section, the TBs generated by the different schemes are compared with the 20ICA simulations. Figures 5 and 6 show the RMS and mean errors for the two different samples. The first thing to note is the order of magnitude difference in the size of the errors between the rainy sample and the clear/cloudy sample. This shows that the errors associated with the simple cloud overlap schemes are essentially restricted to heavy cloud and rainy profiles. Bauer et al. (2006c) and O'Dell et al. (2007) studied these kinds of errors as a function of modeled $C_{\max}$ or precipitation water path; neither of these measures is able to demonstrate such a clear separation between the kind of situations where overlap errors are important and where they are not.

In the rainy sample (Fig. 5), the 2C simulations usually show by far the largest RMS and mean errors. These are worst in channel 37h, with an RMS of 19 K. This channel is particularly sensitive to cloud and rain. Errors are generally larger in the channels that normally have some sensitivity to the surface emission (19v through 50.3 GHz, and 150 ± 1 and 183 ± 7 GHz). The remaining channels (with smaller errors) are sounding channels with weighting functions peaking in the middle or upper troposphere, so they are insensitive to the cloud and rain in the lower parts of the profile. 2C has positive biases of between 3 and 12 K in the lower-frequency channels 19v/h and 37v/h. This is consistent with our hypothesis that, through the use of $C_{\max}$, the 2C approach will give excessive weight to the cloudy part of the grid box. At these frequencies, where emission from rain and cloud produces warmer TBs than the surface, this excessive weight produces TBs much higher than the more accurate 20ICA. Similarly, in channels at 85, 150, and 183 GHz, where cloudy TBs can often be lower than in clear sky [as a result of scattering from snow and cloud ice, or cloud water absorption in relatively cold clouds; e.g., Lin et al. (1998)], the 2C approach underestimates TBs relative to 20ICA.

The use of a weighted mean cloud fraction in the 2R scheme substantially improves agreement with 20ICA, both in terms of mean and RMS. Although it slightly overcompensates in terms of bias, particularly in channels 37v, 37h, and 150 ± 1 GHz, the net effect is still that 2R is much more accurate than 2C. Averaged over all the channels tested, 2R reduces RMS errors by 40% relative to 2C.

The benefits of using two carefully chosen scattering calculations instead of one are shown by the 2O scheme, which generally shows RMS errors much smaller than 2 K. O'Dell et al. (2007) have already demonstrated that this scheme is capable of nearly matching the results of ICA simulations.

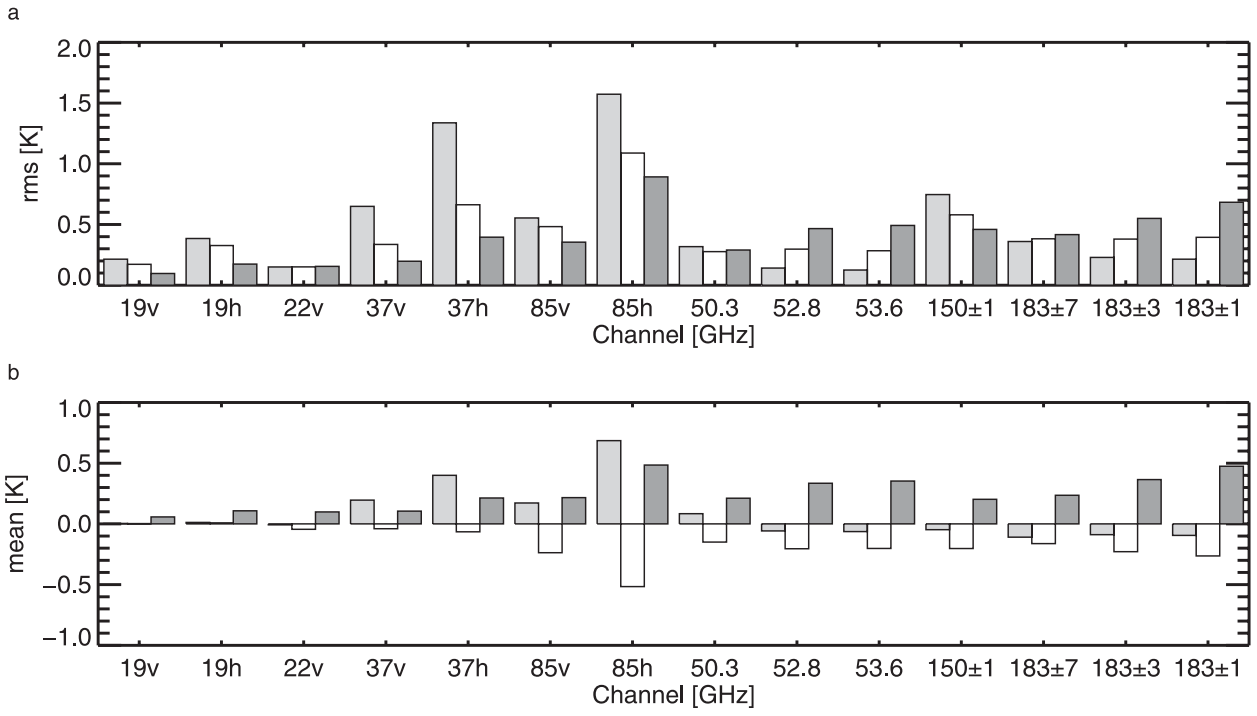

FIG. 6. As in Fig. 5, but showing the clear- and cloudy-sky sample.

The clear- and cloudy-sky sample (Fig. 6) shows much smaller pronounced differences between the cloud overlap schemes. 2C still generally gives the highest RMS errors in surface-sensitive channels, and 2O gives the least. However, in channels with mid- and upper-tropospheric weighting functions (52.8, 53.6, 183 ± 3, and 183 ± 1 GHz), the order reverses. Remember that the optimal column selection of O'Dell et al. (2007) is based on the 37-GHz optical depth as a proxy for TB; as they acknowledge, it is optimized toward the low-frequency imaging channels. This confirms what was discussed earlier, that future improvements should be made by using a different proxy variable at different frequencies to be more representative of the actual radiative transfer.

The 2R scheme also creates slightly larger errors in the mid- and upper-tropospheric sounding channels, but not to the extent of 2O. Again, for better results, C_{tot} should perhaps vary with frequency, and for these sounding channels it should be weighted toward mid- and/or upper-tropospheric cloud and precipitation. Note, however, that the absolute scale of the problem is not that large: for example, at 52.8 GHz the RMS error is 0.12 K for the 2C scheme, compared to 0.28 K for 2R. As will be shown in the next section, such small errors start to become of secondary importance in data assimilation, where the errors in the first guess forecasts can be on the order of several kelvins or more when represented in observation space.

b. SSM/I observations as truth

This section examines observation minus forecast (or departure) statistics for the different cloud overlap schemes. As mentioned before, SSMIS observations were not available at ECMWF in a form suitable for cloud and rain data assimilation, so we compare to observations for the SSM/I channels only. It is common in data assimilation to find systematic biases between model and observations. The mean bias

$$b = \overline{T_{\text{obs}} - T_{\text{sim}}} \tag{9}$$

has been calculated from the observed and simulated TBs T_{obs} and T_{sim}, respectively, including all observations in the region from 40°S to 60°N. Here, T_{sim} is taken from what we believe to be the most accurate simulation, 20ICA. Results are calculated separately for each channel and are given in Table 3.

We remove these biases to prevent them inflating our RMS statistics, so that in the following figures we are looking at the statistics of bias-corrected departures d_k as follows:

$$d_k = T^k_{\text{obs}} - b - T^K_{\text{sim}}, \tag{10}$$

where k is an index for a single observation. The correction does no more than remove the "global" offset between ECMWF and observed TBs.

TABLE 3. SSM/I observation minus ECMWF 20ICA FG averaged over 40°S–60°N during 1–20 Aug 2007.

Channel	Bias b (K)
19v	−1.05
19h	−1.30
22v	1.20
37v	−2.66
37h	−1.13
85v	−0.84
85h	0.45

In the rainy sample (Fig. 7), 2C again stands out as generally having the highest RMS and mean errors. However, it is hard to tell between the three more accurate cloud overlap schemes. When compared with observations, they generally reduce the RMS error, but their performance appears roughly equivalent. The best improvement is seen in channel 85v, where RMS errors are 21 K for the 2C scheme and 13 K for 2R. As seen in comparisons with 20ICA, a limitation with the 2R scheme, particularly at 37 GHz, is that the bias is not always reduced and actually reverses in sign.

The clear and cloudy sample (Fig. 8) shows little differentiation between any of the schemes at the lower frequencies. But, at the higher frequencies, with greater sensitivity to cloud water, snow, and ice, the three ''improved'' schemes do slightly better than 2C.

To examine the issues of bias in more detail, Figs. 9 and 10 show the departures (d_k) binned and averaged by latitude and longitude for channels 19v and 37h, respectively. 2O is omitted because it produces extremely similar results to 20ICA. There is a positive bias poleward of 40°S that is present at both frequencies, no matter which overlap scheme is used. This is not yet fully understood, but it has been a long-standing feature of the first-guess departures at ECMWF. The problem is hypothesized to be a combination of 1) deficiencies in the surface emissivity model at lower temperatures (these problems are much worse in the horizontally polarized channels) and 2) a lack of water cloud and a corresponding surplus of ice cloud in the ECMWF model in cold air masses coming from the Antarctic. Hence, these issues are independent of the cloud overlap problem we are discussing here; as already mentioned, we have eliminated this area from all calculations in this study.

The problem of excess weighting toward the cloudy column in the 2C scheme is clear in Figs. 9a and 10a; simulated TBs are excessively high in the ITCZ and in other regions where clouds and rain are prevalent, such as the storm tracks. Both 2R and 20ICA correct this problem, so that departures are close to zero in much of the ITCZ and storm tracks. However, an area of positive departures has appeared over the Maritime Continent in

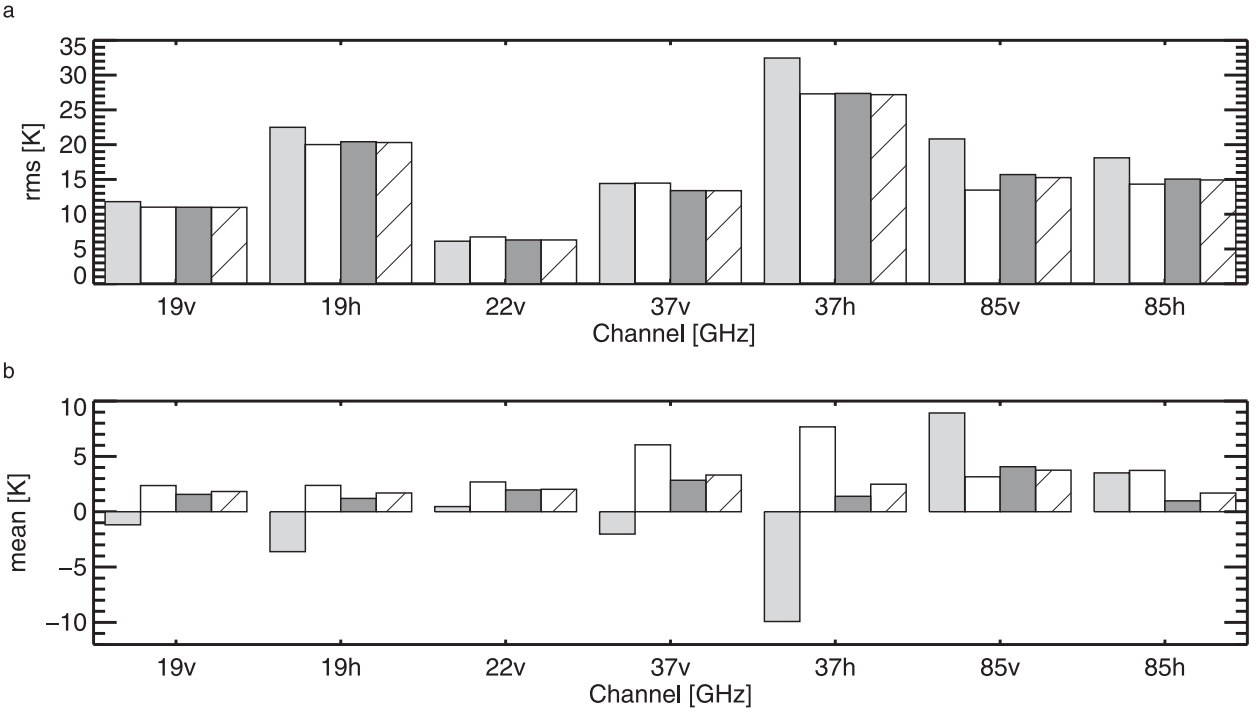

FIG. 7. (a) RMS and (b) mean bias-corrected departures in 2C (light gray), 2R (white), 2O (dark gray), and 20ICA (stripes) simulated TBs, as compared with the SSM/I observations, for the rainy-sky sample.

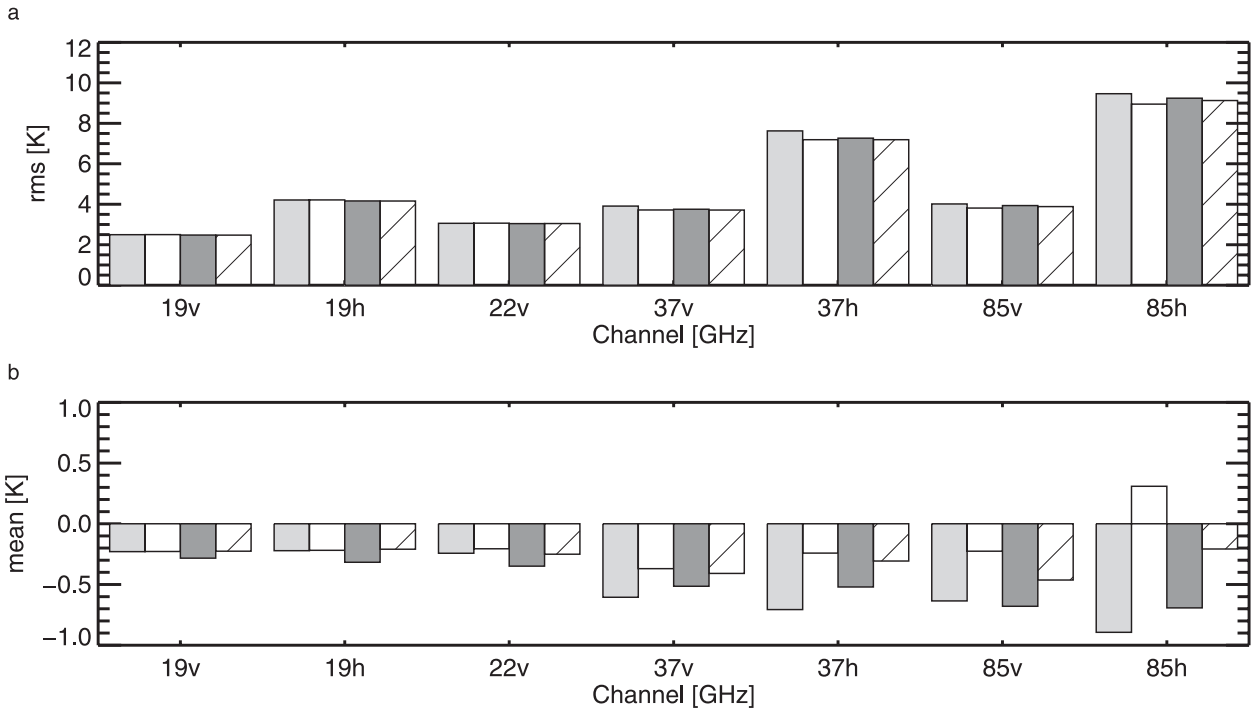

FIG. 8. As in Fig. 7, but for the clear- and cloudy-sky sample.

both 2R and 20ICA. In channel 19v, given that the feature appears even with the accurate 20ICA, this may indicate a problem with the ECMWF model itself, perhaps producing too little rain in this region and at this time of year (August 2007). In channel 37h, the Maritime Continent departures are somewhat larger for 2R than for 20ICA, and this exemplifies the overcompensation problem we have already noted in the 2R scheme, which is most problematic in the 37-GHz channels. Overall, however, the 2R scheme gives a very large reduction in the size of the tropical bias relative to 2C, and does nearly as well as 20ICA.

5. Conclusions

It was suspected that biases in simulated SSM/I TBs in cloud- and rain-affected data assimilation at ECMWF were coming from a flawed cloud overlap scheme in the RTTOV-SCATT radiative transfer model. Bauer et al. (2006c) acknowledged that the cloud overlap treatment originally used in RTTOV-SCATT (referred to as 2C) was one of the areas of largest uncertainty. O'Dell et al. (2007) demonstrated that SSM/I first-guess departures could be reduced by using a multiple-independent column approach with maximum-random overlap (20ICA). They also presented an optimal cloud overlap scheme (2O) that showed very good results in comparison with multiple independent column simulations. However, neither of these approaches can yet be used in operational data assimilation at ECMWF because they are too computationally expensive. This paper introduces a simple revision to the RTTOV-SCATT cloud overlap, referred to as 2R, which substantially improves agreement with observations and more accurate models with no extra computational cost.

Comparisons have been made in the context of the ECMWF NWP system, which has been used to generate a sample of 4.2 million profiles for the period 1–20 August 2007. A total of 463 093 of these are affected by rain or heavy cloud in either model or observation, as identified by the 37-GHz polarization difference. It has been shown that the principal limitation of the original RTTOV-SCATT overlap scheme was the use of the maximum cloud fraction when partitioning between its clear and cloudy columns. By using a hydrometeor-weighted average cloud fraction instead, errors are substantially reduced. RMS errors are on average 40% lower in 2R than 2C when compared to accurate 20ICA simulations in areas of rain or heavy cloud. The new cloud overlap shows reasonable improvement for both imaging and sounding channels, all the way from low (e.g., 19 GHz) to high (e.g., 183 GHz) microwave frequencies. A minor problem is a slight increase in bias in light cloud conditions in the mid- and upper-tropospheric sounding channels. Improving the situation in the future would require a frequency-dependent cloud overlap.

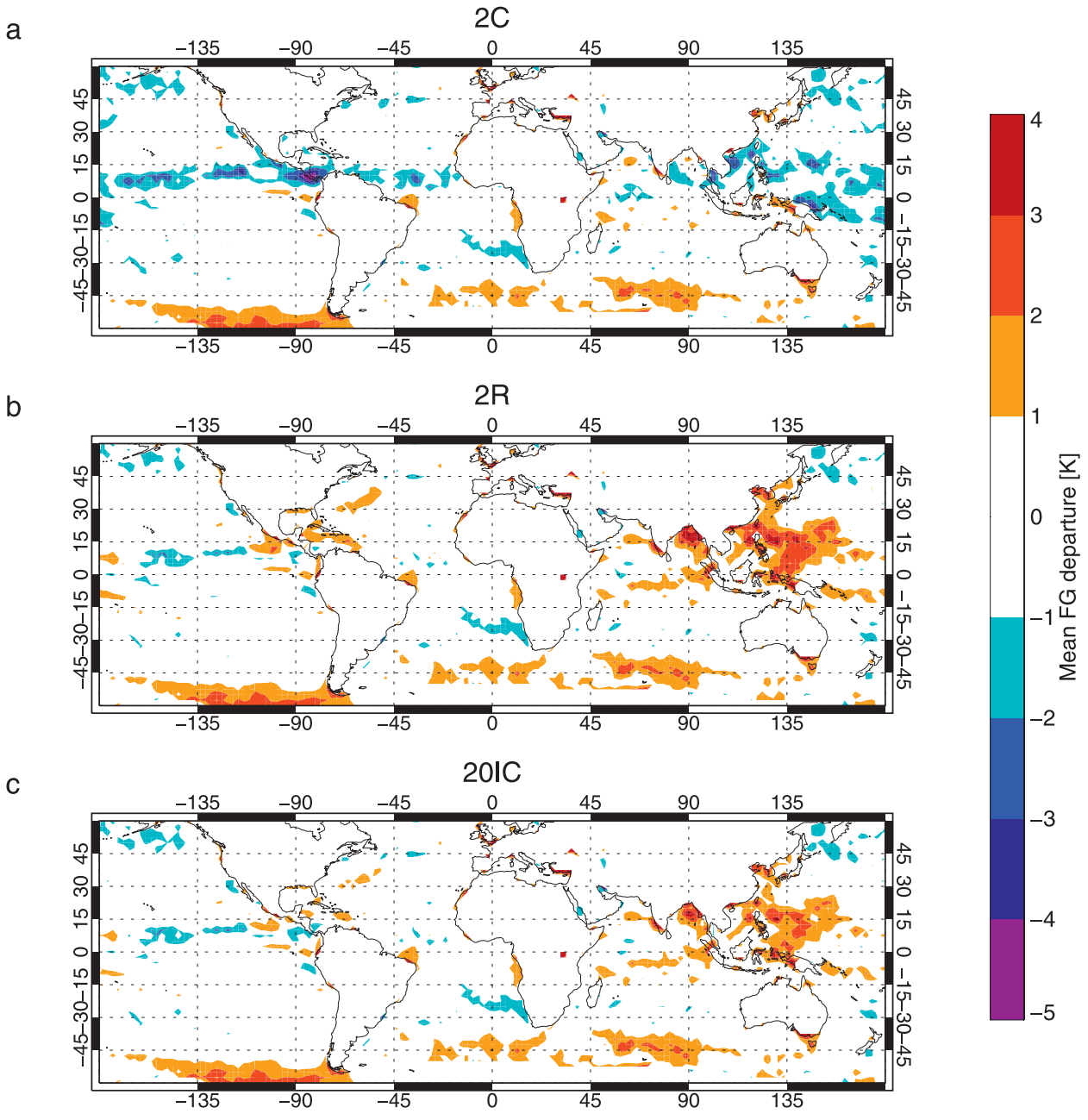

FIG. 9. Mean bias-corrected departures for SSM/I channel 19v for (a) 2C, (b) 2R, and (c) 20ICA, binned in 2.5° × 2.5° boxes.

In terms of RMS errors compared to observations, all three new overlap schemes (2R, 2O, and 20ICA) improve substantially on the performance of the 2C scheme in areas of rain or heavy cloud. For example, RMS errors are reduced from 22.5 to 20 K in channel 19h and from 21 to 13 K in channel 85v. However, all three schemes show a very similar performance, with the exception that 2R slightly underpredicts TBs over the Maritime Continent. The impact on observation statistics is small in clear and less heavily cloudy areas. The results for 2R are good enough that it will be used operationally at ECMWF in the near future, and it will also be included as an option in version 9.3 of RTTOV-SCATT.

The fact that the new overlap scheme largely removes biases in rainy and cloudy areas is particularly important in the context of data assimilation. This bias would have been difficult to control using the standard bias correction approaches, and biases between model and observations can lead to problems such as the precipitation

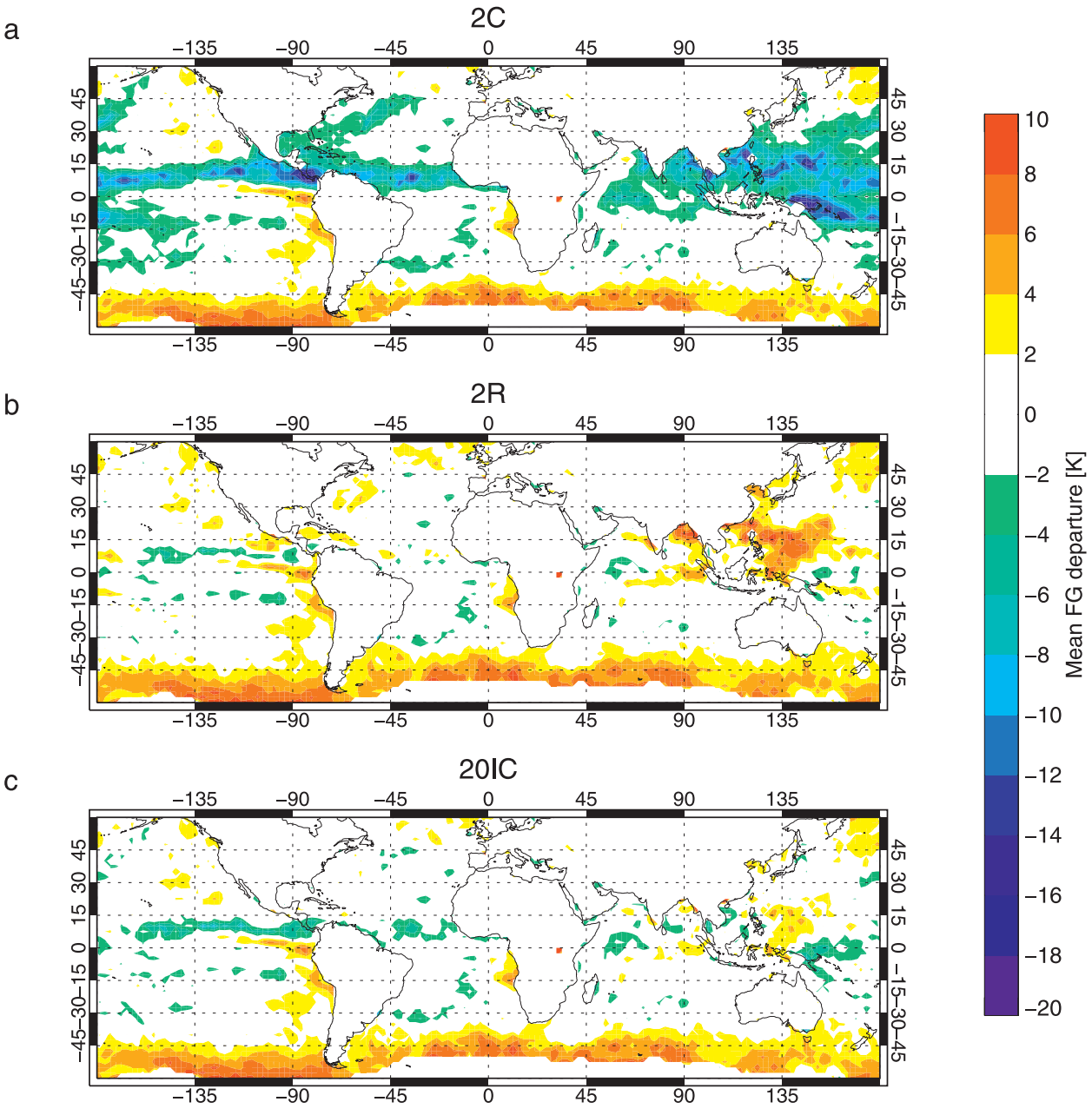

FIG. 10. As in Fig. 9, but for channel 37h.

spindown experienced in the 40-yr ECMWF Re-Analysis (ERA-40; Uppala et al. 2005).

We have also seen that the optimal cloud overlap scheme of O'Dell et al. (2007) shows levels of error that are very similar to that of the multiple independent column approach (20ICA). It would be around 80%–100% more computationally expensive than 2C or 2R if implemented in RTTOV-SCATT, but it should be a long-term goal to do this and to start using it for operational assimilation. However, the scheme currently uses 37-GHz optical depth to optimize the cloud overlap calculations. This appears to increase RMS errors compared to 20ICA in the 50- and 183-GHz sounding channels. Here, as for the 2R scheme, the cloud overlap would need to be optimized to be more representative of the radiative transfer at these frequencies.

Finally, we note that the assimilation of rain and cloud observations is getting to the point where we can start to identify possible problems in cloud and rain in the ECMWF model. In the August 2007 comparisons using the accurate 20ICA radiative transfer, we have seen 1) a positive bias over the Maritime Continent, which could

be explained by an underprediction of column rain amounts there, and 2) a positive bias in the Southern Ocean, which could be partly explained by an excess of cloud ice, as compared with cloud water, in cold air masses coming from the Antarctic. The surface emissivity scheme is also likely to be a factor here. However, further work would be required to confirm these hypotheses.

Acknowledgments. Alan Geer's work at ECMWF was funded through an EUMETSAT research fellowship. Philippe Bougeault, Jean-Jacques Morcrette, and Jean-Noël Thépaut are thanked for reviewing the manuscript prior to submission. The anonymous referees are thanked for their helpful suggestions.

REFERENCES

Barker, H., 2008: Overlap of fractional cloud for radiation calculations in GCMs: A global analysis using CloudSat and CALIPSO data. *J. Geophys. Res.,* **113,** D00A01, doi:10.1029/2007JD009677.

Bauer, P., P. Lopez, A. Benedetti, D. Salmond, and E. Moreau, 2006a: Implementation of 1D+4D-Var assimilation of precipitation-affected microwave radiances at ECMWF. I: 1D-Var. *Quart. J. Roy. Meteor. Soc.,* **132,** 2277–2306.

——, ——, D. Salmond, A. Benedetti, S. Saarinen, and E. Moreau, 2006b: Implementation of 1D+4D-Var assimilation of precipitation-affected microwave radiances at ECMWF. II: 4D-Var. *Quart. J. Roy. Meteor. Soc.,* **132,** 2307–2332.

——, E. Moreau, F. Chevallier, and U. O'Keeffe, 2006c: Multiple-scattering microwave radiative transfer for data assimilation applications. *Quart. J. Roy. Meteor. Soc.,* **132,** 1259–1281.

Bell, W., and Coauthors, 2008: The assimilation of SSMIS radiances in numerical weather prediction models. *IEEE Trans. Geosci. Remote Sens.,* **46,** 884–900.

Chevallier, F., and P. Bauer, 2003: Model rain and clouds over oceans: Comparison with SSM/I observations. *Mon. Wea. Rev.,* **131,** 1240–1255.

Colton, M. C., and G. A. Poe, 1999: Intersensor calibration of DMSP SSM/I's: F-8 to F-14, 1987–1997. *IEEE Trans. Geosci. Remote Sens.,* **37,** 418–439.

Deblonde, G., J.-F. Mahfouf, B. Bilodeau, and D. Anselmo, 2007: One-dimensional variational data assimilation of SSM/I observations in rainy atmospheres at MSC. *Mon. Wea. Rev.,* **135,** 152–172.

Eyre, J. R., 1991: A fast radiative transfer model for satellite sounding systems. ECMWF Tech. Memo. 176.

Geer, A. J., P. Bauer, and P. Lopez, 2008: Lessons learnt from the operational 1D+4D-Var assimilation of rain- and cloud-affected SSM/I observations at ECMWF. *Quart. J. Roy. Meteor. Soc.,* **134,** 1513–1525.

Geleyn, J. F., and A. Hollingsworth, 1979: An economical analytical method for the computation of the interaction between scattering and line absorption of radiation. *Contrib. Atmos. Phys.,* **52,** 1–16.

Hogan, R. J., and A. J. Illingworth, 2000: Deriving cloud overlap statistics from radar. *Quart. J. Roy. Meteor. Soc.,* **126,** 2903–2909.

Hollinger, J., J. Peirce, and G. Poe, 1990: SSM/I instrument evaluation. *IEEE Trans. Geosci. Remote Sens.,* **28,** 781–790.

Joseph, J., W. J. Wiscombe, and J. A. Weinman, 1976: The delta-Eddington approximation for radiative flux transfer. *J. Atmos. Sci.,* **33,** 2452–2459.

Karstens, U., C. Simmer, and E. Ruprecht, 1994: Remote sensing of cloud liquid water. *Meteor. Atmos. Phys.,* **54,** 157–171.

Kelly, G. A., P. Bauer, A. J. Geer, P. Lopez, and J.-N. Thépaut, 2008: Impact of SSM/I observations related to moisture, clouds, and precipitation on global NWP forecast skill. *Mon. Wea. Rev.,* **136,** 2713–2726.

Kummerow, C., 1998: Beamfilling errors in passive microwave rainfall retrievals. *J. Appl. Meteor.,* **37,** 356–370.

Kunkee, D., G. Poe, D. Boucher, S. Swadley, Y. Hong, J. Wessel, and E. Uliana, 2008: Design and evaluation of the first Special Sensor Microwave Imager/Sounder. *IEEE Trans. Geosci. Remote Sens.,* **46,** 863–883.

Lin, B., B. Wielicki, P. Minnis, and W. Rossow, 1998: Estimation of water cloud properties from satellite microwave, infrared, and visible measurements in oceanic environments: 1. Microwave brightness temperature simulations. *J. Geophys. Res.,* **103,** 3873–3886.

Mace, G. G., and S. Benson-Troth, 2002: Cloud-layer overlap characteristics derived from long-term cloud radar data. *J. Climate,* **15,** 2505–2515.

Morcrette, J.-J., and Y. Fouquart, 1986: The overlapping of cloud layers in shortwave radiation parametrizations. *J. Atmos. Sci.,* **43,** 321–328.

——, and C. Jakob, 2000: The response of the ECMWF model to changes in the cloud overlap assumptions. *Mon. Wea. Rev.,* **128,** 1707–1732.

——, H. Barker, J. Cole, M. Iacono, and R. Pincus, 2008: Impact of a new radiation package, McRad, in the ECMWF integrated forecasting system. *Mon. Wea. Rev.,* **136,** 4773–4798.

Naud, C., A. D. Genio, G. Mace, S. Benson, E. Clothiaux, and P. Kollias, 2008: Impact of dynamics and atmospheric state on cloud vertical overlap. *J. Climate,* **21,** 1758–1770.

O'Dell, C. W., P. Bauer, and R. Bennartz, 2007: A fast cloud overlap parametrization for microwave radiance assimilation. *J. Atmos. Sci.,* **64,** 3896–3909.

Petty, G., 1994: Physical retrievals of over-ocean rain rate from multichannel microwave imagery. Part I: Theoretical characteristics of the normalized polarization and scattering indices. *Meteor. Atmos. Phys.,* **54,** 79–99.

Pincus, R., H. Barker, and J.-J. Morcrette, 2003: A fast, flexible, approximate technique for computing radiative transfer in inhomogeneous cloud fields. *J. Geophys. Res.,* **108,** 4376, doi:10.1029/2002JD003322.

Rabier, F., H. Järvinen, E. Klinker, J.-F. Mahfouf, and A. Simmons, 2000: The ECMWF operational implementation of four-dimensional variational assimilation. I: Experimental results with simplified physics. *Quart. J. Roy. Meteor. Soc.,* **126,** 1148–1170.

Saunders, R., 2008: RTTOV-9 science and validation report. NWP-SAF Rep. NWPSAF-MO-TV-020, 74 pp.

Smith, E. A., P. Bauer, F. S. Marzano, C. D. Kummerow, D. McKague, A. Mugnai, and G. Panegrossi, 2002: Intercomparison of microwave radiative transfer models for precipitating clouds. *IEEE Trans. Geosci. Remote Sens.,* **40,** 541–549.

Uppala, S. M., and Coauthors, 2005: The ERA-40 Re-Analysis. *Quart. J. Roy. Meteor. Soc.,* **131,** 2961–3012.

Weinman, J. A., and R. Davies, 1978: Thermal microwave radiances from horizontally finite clouds of hydrometeors. *J. Geophys. Res.,* **83** (C6), 3099–3107.